BNL-108608-2015-JA

Comparing Highly Ordered Monolayers of Nanoparticles Fabricated Using Electrophoretic Deposition: Cobalt Ferrite Nanoparticles versus Iron Oxide Nanoparticles

Authors: Alex J. Krejci[1,2,3], Adriana-Mendoza Garcia[4], Shouheng Sun[4], James H. Dickerson[5,6]

[1]Department of Mechanical Engineering, SUNY Korea, 119 Songdo Moonhwa-Ro, Incheon 406-840, South Korea

[2]Department of Computer Science, SUNY Korea, 119 Songdo Moonhwa, Ro, Incheon 406-840 South Korea

[3]Department of Mechanical Engineering, Stony Brook University, Stony Brook, New York, 11794, USA

[4]Department of Chemistry, Brown University, Providence, RI 02912, USA

[5]Department of Physics, Brown University, Providence, RI 02912, USA

[6]Center for Functional Nanomaterials, Brookhaven National Laboratory, Upton, NY 11973, USA

Ordered assemblies of nanoparticles remain challenging to fabricate, yet could open the door to many potential applications of nanomaterials. Here, we demonstrate that locally ordered arrays of nanoparticles, using electrophoretic deposition, can be extended to produce long-range order among the constituents. Voronoi tessellations along with multiple statistical analyses show dramatic increases in order compared with previously reported assemblies formed through electric field-assisted assembly. Based on subsequent physical measurements of the nanoparticles and the deposition system, the underlying mechanisms that generate increased order are inferred.

I. Introduction:

Ordered systems of nanoparticles (superlattices) have attracted interest in the research and industry due to their potential application in a wide variety of devices.[1–4] Many emerging techniques have been proposed to fabricate these superlattices, including evaporative self-assembly, spin-casting, and ligand-mediated self-assembly, and more recently, electrophoretic deposition [5–8]. The eventual applicability of nanoparticle (NP) superlattices in a device depends on how well arranged (ordered, glassy, disordered, etc.) the constituent particles are, how cost-effective the process to produce the array is, and how dependent the proposed device applications are on the existing order[9]. Comparably, just as macroscopic crystals behave differently from their amorphous counter parts, and the spectrum of atomic arrangement of amorphous to perfect crystalline has a continuum of properties, similar phenomena occur for supercrystals[3]. The degree of ordering of supercrystals can deeply affect the physical characteristics of the supercrystals and, thus, the applications in which they may be incorporated.

Electrophoretic deposition (EPD) is an advantageous technique for the assembly of nanoparticles because of its ease of application, scalability, and rapid performance [10–16]. A recently developed EPD technique has been able to create locally ordered monolayers of NPs[17–19]. Understanding the mechanisms that create the ordering could allow one to tune the ordering to create supercrystals using EPD. In this light, recently developed statistical measurement tools have been demonstrated to be effective in quantifying the degree of ordering within monolayers of nanoparticles[20,21]. Motivated by this work, this article explores the application of these tools to two different systems (iron oxide and cobalt ferrite nanoparticles) and the observation of markedly different degrees of order in the systems. Based on physical measurements of the NP systems, the mechanisms behind the ordering in each system are deduced.

II. Experiment

Suspension Preparation and Characterization: Cobalt Ferrite NPs were synthesized via a modified process of the thermal decomposition of $Fe(acac)_3$ and $Co(acac)_2$ in benzyl ether (BE), where acac is acetylacetonate [22]. A solution of $Fe(acac)_3$ (1.0 mmol), $Co(acac)_2$ (0.5 mmol), OAc (2 mL), OAm (3 mL) and BE (20 mL) in a four-neck flask was magnetically stirred under a flow of argon (Ar) and heated up to 120 °C for 30 min, where OAm is Oleylamine and OAc is Oleic Acid. Under an Ar blanket, the solution was further heated up to 210 °C at a heating rate of 3 °C /min and kept at this temperature for 2 h. Finally, the mixture was heated up to 300 °C, at the same heating rate, and kept at this temperature for 1.5 h. NPs were collected and washed by addition of ethanol (20 ml) and subsequent centrifugation at 9000 rpm for 8 min. The product was finally re-suspended in hexane. Iron oxide NPs were synthesized using a thermal decomposition approach, as described elsewhere [23,17]. Iron oxide NPs were cleaned using a similar centrifugation algorithm using butanol and ethanol and re-suspended in hexane.

Nanoparticle Characterization: Both NP types were characterized for crystallinity, size, and magnetic properties using x-ray diffraction (XRD), transmission electron microscopy (TEM), dynamic light scattering, and magnetic hysteresis measurements. Absorption measurements of iron oxide were also performed to affirm the composition (γ-Fe_2O_3 or Fe_3O_4) of the nanoparticles. XRD measurements confirm that the cobalt ferrite NPs were in the inverse spinel crystal structure with a lattice parameter similar to that of magnetite. TEM measurements show that cobalt ferrite NPs were monodisperse, single crystalline, spherical, and had an average diameter of 12.2 ± 0.8 nm. Magnetic hysteresis measurements indicated ferromagnetic behavior of the NPs with a magnetic moment of ~26,000μ_B per NP (Figure 2). The hydrodynamic diameters of the re-suspended NPs were measured using dynamic light scattering, resulting in a similar size for both NPs: 10.8 nm for iron oxide and 12.3 nm for cobalt ferrite (Figure 1a). The mobilities of the NPs were also measured, indicating the iron oxide NP suspension had NPs with both positive and negative mobility, while the cobalt ferrite suspension had NPs with a mostly negative mobility (Figure 1b). Iron oxide NPs were characterized previously, and displayed single crystalline inverse spinel structure, monodispersity, and a spherical shape with an average diameter of 9.6 ± 0.9 nm.[21] Iron oxide NPs behaved paramagnetically with a magnetic moment of 1800μ_B per NP.

Electrophoretic Deposition: The cobalt ferrite and iron oxide NPs were deposited onto epi-ready, phosphorus-doped, silicon wafers with an extant native oxide surface layer. EPD was performed by first mounting two silicon wafers, acting as electrodes, 5 mm apart in parallel plate capacitor configuration. The electrode sizes were ~5 mm X 50 mm, and were inserted into the nanoparticle suspension to a depth of ~30 mm. A voltage of 50 V was applied across the electrodes for 60 s, then the electrodes were extracted from the NP suspension. After another 60 s, the voltage was turned off.

Film Characterization: The resulting NP films were imaged using a Hitachi S-4800 scanning electron microscope (SEM). MATLAB was used to process the images by first locating regions with no deposition then locate each particle in the film.[21] Using the location data, Voronoi tessellations were constructed and statistical analyses were performed.[20] All analyses were performed on images of at least five regions of each film.

III. Results

SEM images of NP monolayers overlaid with Voronoi tessellations are shown Figure 3. Figure 3a shows iron oxide monolayers with small regions of hexagonal ordering and many defects. Figure 3b shows the same image with Voronoi tessellations only for those particles considered well-ordered.[20] In this figure, the color indicates the orientation of the hexagonal cell. From these two images, only small clusters of well-ordered iron oxide NPs were visible. Furthermore, neighboring well-ordered clusters more likely presented different orientations than not, indicating that the correlation length in the film was quite low. In general, too many defects existed in these systems for a large degree of ordering to have developed.

Complementary images of the cobalt ferrite NP films appear to be substantially different. Figure 3c shows that most of the nanoparticles packed into hexagonally arrayed monolayers. Figure 3d confirms that the regions are highly correlated. Large clusters of oriented particles exist, and sharp transitions in the orientation of neighboring clusters are observed. In this system, a clear correlation exists between two NPs that are separated by up to ~20 NP diameters. Also noted is the large difference in void patterns between the iron oxide and cobalt ferrite. In the iron oxide film, voids tend to be frequent and small, whereas the cobalt ferrite film exhibited few but larger voids for comparable film densities.

Quantifying the degree of order, drastic differences were observed. In measuring the Voronoi-cell edge-fraction distribution (Figure 4a), a very strong peak (~85%) was observed at n=6 for cobalt ferrite, and a relatively weak peak (~55%) for iron oxide. The local bond-orientation order parameter distribution indicated a high degree of order in cobalt ferrite, with the peak intensity pushing toward the right side of the graph (Figure 4b). Further, the radial distribution function showed peaks even at distances greater than four NP separation for cobalt ferrite. For iron oxide, the distribution flattens at less than a three NP center-to-center spacings (Figure 4c).

IV. Discussion

Such drastic differences in order are indicative of differing mechanisms that cause ordering. Iron oxide ordering was previously observed to occur only after deposition and after the films had been extracted from the solvent.[19] From these observations, capillary forces were inferred to have assisted in drawing the NPs together into local regions of hexagonal packing. To consider what forces may be involved in attracting the NPs toward each other, the magnitude of the magnetic interactions were explored. By obtaining magnetic moments of the NPs based on hysteresis measurements and TEM measurement, combined with NP-NP spacing measurement based on the NP film, the magnetic dipole-dipole interactions between neighboring NPs were calculated. Presuming a head-to-tail (i.e. tandem) orientation of the magnetic moments between neighboring iron oxide NPs, this energy was $-0.005\ \mathrm{k}_B\mathrm{T}$. For cobalt ferrite NPs, the magnetic interaction energy was $-0.8\ \mathrm{k}_B\mathrm{T}$.[21] While the dipole-dipole interaction energy is less than thermal energy at room temperature, the cobalt ferrite NP monolayer

was very likely affected by collective magnetic interactions between the NPs. The differences in ordering coupled with the two orders of magnitude difference in the energy of the associated magnetic interactions between cobalt ferrite NPs and iron oxide NPs strongly suggests that magnetic interactions are a primary driver in the increased order.

Based on these observations, a process emerged for the deposition that could explain the observed ordering in cobalt ferrite NP monolayers. First, the applied electric field drives cobalt ferrite NPs toward the electrode through electrophoresis. Drag forces between the NPs and the surrounding hexane media cause the NPs to reach readily a terminal velocity, a value that can be estimated from mobility measurements. During the approach toward the substrate, NPs exhibit both translational and rotational Brownian motion; thus, the orientation of the magnetic moment of the NP is constantly changing.[24,25] In the dilute suspensions, spacing between NPs is large, so NP-NP interactions are minimal. Initially, the first few particles deposit randomly on the surface of the substrate. Then, as more particle approach the substrate, the NPs are magnetically attracted toward those NPs already on the substrate. The magnetic moment of the two NPs then becomes fixed to maintain their attractive interaction. As more NPs deposit, small islands begin to form on the surface. These islands exhibit a high degree of ordering. Eventually, these small islands begin to merge producing line defects in the NP film. These line defects are observed in the Figure 3c as where lines of typically 5-sided and 7-sided Voronoi cells. Crossing this line is accompanied with a sharp transition in the orientation of the hexagonal packing, as expected by films generated via island growth. After islands merge, large openings in the monolayer remain because newly deposited NPs are magnetically attracted to the large layer of previously deposited NPs.

V. Conclusions:

Iron oxide and cobalt ferrite NP monolayers fabricated via EPD exhibit notably different degrees of ordering, with cobalt ferrite NPs exhibiting a highly ordered structure. This ordering is likely due to magnetic interactions between cobalt ferrite NPs, having dipole-dipole interaction energy near the thermal energy. On the other hand, the iron oxide magnetic dipole-dipole interaction is much less than thermal energy. Based on the film morphology, a process of deposition is hypothesized. However, certain aspects of this process remain uncertain and could be more deeply addressed using computational modelling. For example, determining whether the NPs are still mobile once they contact the surface of the substrate is a challenge. Studies of iron oxide NPs suggest that limited mobility is still available, as ordering occurs after deposition.[19] Still, it is uncertain whether particles could traverse distances of >8 NP diameters (size of voids in the cobalt ferrite films) after interacting with the substrate. Additionally, if magnetic interactions are driving the ordering, the nanoparticles should have aligned crystal structures. If the magnetic moments of the NPs are aligned, then the easy crystalline axis of the NPs should also be aligned. Such alignment is detectable using XRD. XRD measurements along with modelling of the NP behavior during EPD could provide answers to both of these questions. Such future studies can give a more complete understanding of the deposition process, making it possible to tune the ordering and behavior of the NP monolayer films.

Additionally, as the variety of NP chemistries and geometries that can be deposited as NP monolayers increases, understanding mechanisms of ordering and behaviors of deposition will become a very powerful tool to create finely tuned films. Once ordering in the monolayer is understood well, this technique could be used to create ordered 3D supercrystals.

VI. Acknowledgements:

This research was supported by the United States National Science Foundation Awards DMR-1054161 and DMR-1361068. "This research used resources of the Center for Functional Nanomaterials, which is a U.S. DOE Office of Science Facility, at Brookhaven National Laboratory under Contract No. DE-SC0012704.

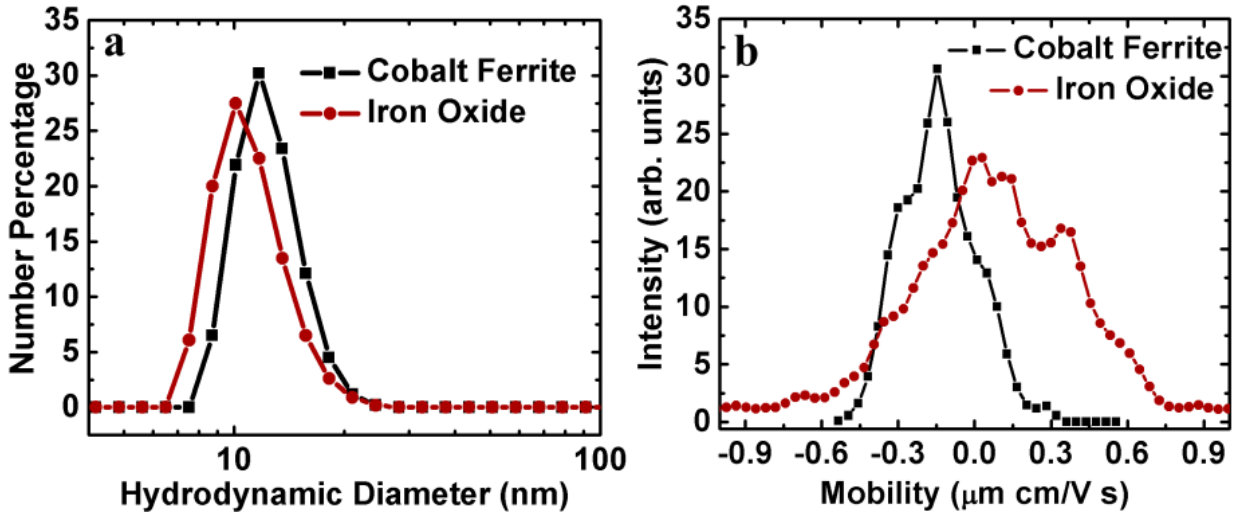

Figure 1: (a) Dynamic light scattering measurements show similar hydrodynamic sizes of cobalt ferrite and iron oxide NPs, and also indicate the NPs were monodisperse in the suspension. (b) Mobility measurements show that iron oxide NPs had both positive and negative mobility, while cobalt ferrite had mostly negative mobility.

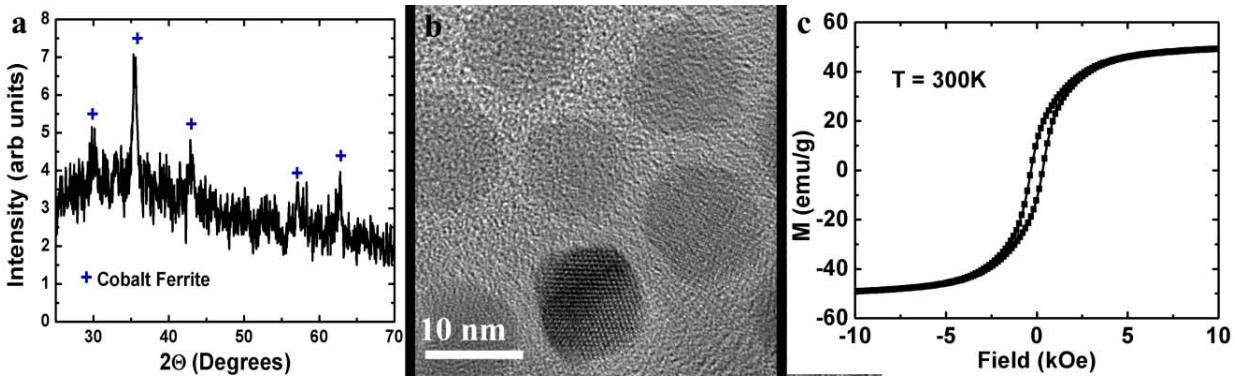

Figure 2: Cobalt ferrite NP characterizations were performed using (a) XRD, (b) TEM, and (c) hysteresis measurements. XRD confirmed an inverse-spinel structure of the NPs. TEMs show monodispersity and observations of lattice structure showed the single-crystal nature of the NPs. Hysteresis showed the NPs behave ferromagnetically.

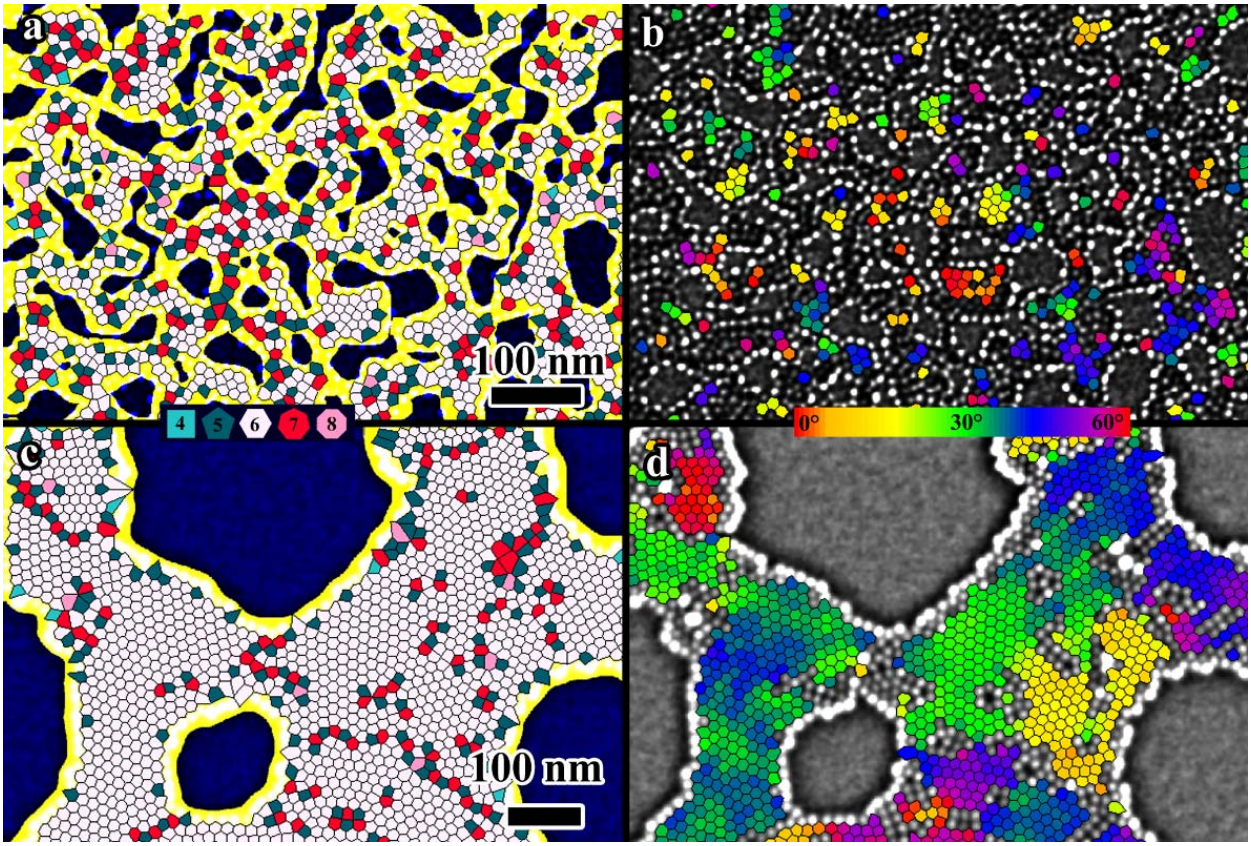

Figure 3: (a) Iron oxide monolayer film imaged using SEM, overlayed with a Voronoi tessellation of the film. Each polygon represents a single particle, the number of neighbors is indicated by the color of the cell. Dark blue regions are voids in the film with no deposition, and yellow regions are particles on the edge of voids for which Voronoi cells were not drawn. (b) The same film as in (a), but with only well-ordered NPs selected. The color of the NPs here represents the orientation of the hexagon (0º meaning a hexagon with vertices on top and bottom). (c) Cobalt ferrite Voronoi tessellation exhibits a much higher degree of ordering than iron oxide NP. (d) The same image as in (c), but now the orientation of the well-ordered cobalt ferrite NPs was observed to be consistent over a long range.

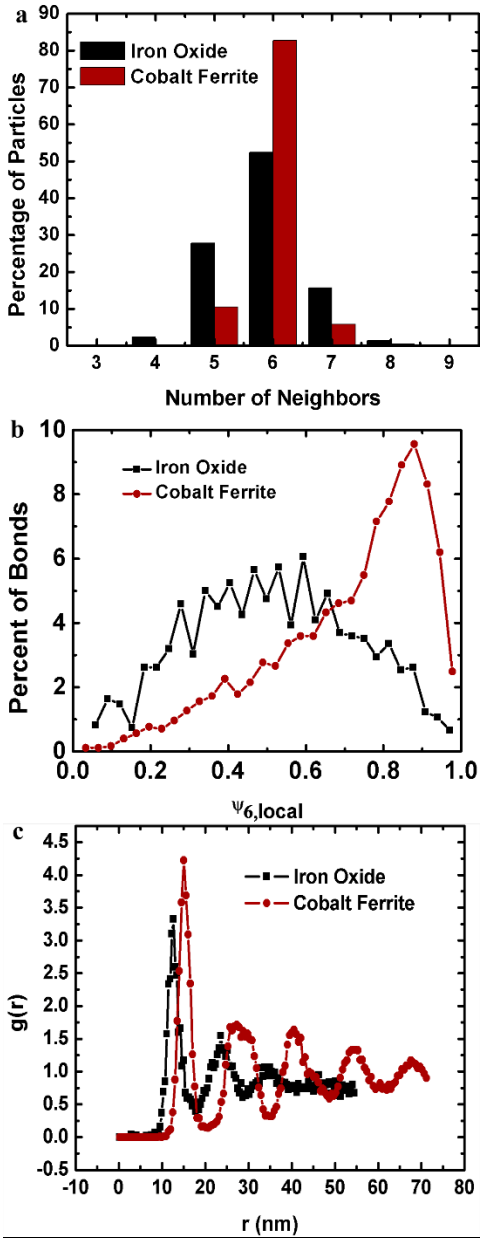

Figure 4: (a) Voronoi-cell edge-fraction distribution shows that cobalt ferrite has many NPs with a high degree of ordering, as many NPs are hexagonally packed (b) The local bond-orientation order-parameter corroborates the data from (a), showing a high percentage of NPs with highly ordered bonding. (c) The radial distribution function shows a high correlation length for cobalt ferrite NPs compared to iron oxide NPs.

References

1. a Courty, a-I. Henry, N. Goubet, and M.-P. Pileni, *Nat. Mater.*, **6**, 900–907 (2007).

2. A. Moser et al., *J. Phys. D. Appl. Phys.*, **35**, R157–R167 (2002).

3. N. Zaitseva, Z. R. Dai, F. R. Leon, and D. Krol, *J. Am. Chem. Soc.*, **127**, 10221–10226 (2005).

4. B. Radha et al., *Nano Lett.*, **14**, 2162–2167 (2014) http://pubs.acs.org/doi/abs/10.1021/nl500473t.

5. E. V Shevchenko, D. V Talapin, N. a Kotov, S. O'Brien, and C. B. Murray, *Nature*, **439**, 55–59 (2006).

6. D. V. Talapin, E. V. Shevchenko, C. B. Murray, A. V. Titov, and P. Král, *Nano Lett.*, **7**, 1213–1219 (2007).

7. S. Y. Park et al., *Nature*, **451**, 553–556 (2008).

8. A. C. Johnston-Peck, J. Wang, and J. B. Tracy, *Langmuir*, **27**, 5040–5046 (2011).

9. Z. Nie, A. Petukhova, and E. Kumacheva, *Nat. Nanotechnol.*, **5**, 15–25 (2010) http://dx.doi.org/10.1038/nnano.2009.453.

10. S. A. Hasan et al., *ACS Nano*, **4**, 7367–7372 (2010).

11. J. L. Rigueur, S. a. Hasan, S. V. Mahajan, and J. H. Dickerson, *Carbon N. Y.*, **48**, 4090–4099 (2010) http://dx.doi.org/10.1016/j.carbon.2010.07.016.

12. I. Gonzalo-Juan, A. J. Krejci, and J. H. Dickerson, *Langmuir*, **28**, 5295–5301 (2012) http://www.ncbi.nlm.nih.gov/pubmed/22352851.

13. S. Somarajan, S. a. Hasan, C. T. Adkins, E. Harth, and J. H. Dickerson, *J. Phys. Chem. B*, **112**, 23–28 (2008).

14. M. a. Islam and I. P. Herman, *Appl. Phys. Lett.*, **80**, 3823–3825 (2002).

15. S. Jia, S. Banerjee, and I. P. Herman, *J. Phys. Chem. C*, **112**, 162–171 (2008).

16. I. Gonzalo-Juan et al., *Green Chem.*, **16**, 3286–3296 (2014).

17. A. J. Krejci, I. Gonzalo-Juan, and J. H. Dickerson, *ACS Appl. Mater. Interfaces*, **3**, 3611–3615 (2011).

18. A. J. Krejci, J. Mandal, and J. H. Dickerson, *Appl. Phys. Lett.*, **101**, 1–5 (2012).

19. A. J. Krejci, K. G. Yager, C. Ruggiero, and J. H. Dickerson, *Nanoscale*, **6**, 4047 (2014) http://xlink.rsc.org/?DOI=c4nr00645c.

20. A. J. Krejci, C. G. W. Thomas, and J. H. Dickerson, *Phys. Rev. E - Stat. Nonlinear, Soft Matter Phys.*, **87**, 1–9 (2013).

21. A. J. Krejci et al., *J. Phys. Chem. B*, **117**, 1664–1669 (2013).

22. Y. Yu, A. Mendoza-Garcia, B. Ning, and S. Sun, *Adv. Mater.*, **25**, 3090–3094 (2013).

23. J. Park et al., *Nat. Mater.*, **3**, 891–895 (2004).

24. J. P. Wang, *Proc. IEEE*, **96**, 1847–1863 (2008).

25. S. H. Chung et al., *Appl. Phys. Lett.*, **85** (2004).

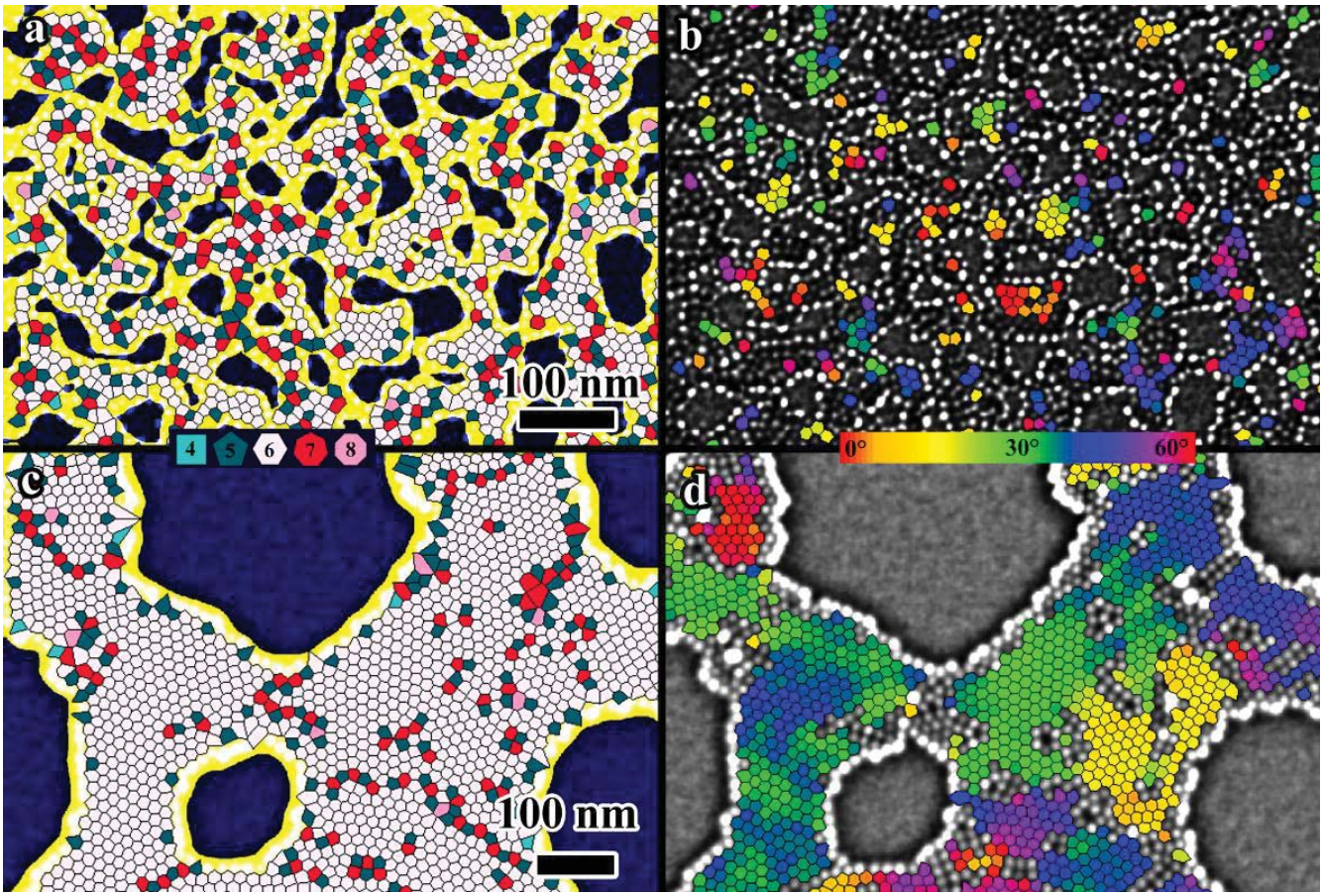
a
b
c
d
100 nm
100 nm
4
5
6
7
8
0°
30°
60°